

# The Line Emission Region in III Zw 2: Kinematics and Variability

L. Č. Popović<sup>1,2,3</sup>, E. G. Mediavilla<sup>4</sup>, E. Bon<sup>1,3</sup>, N. Stanić<sup>1,3</sup> and A. Kubičela<sup>1,3</sup>

<sup>1</sup>*Astronomical Observatory, Volgina 7, 11160 Belgrade 74, Serbia*

<sup>2</sup>*Astrophysikalisches Institut Potsdam, An der Sternwarte 16, 14482 Potsdam, Germany  
(Alexander von Humboldt Fellow)*

<sup>3</sup>*Isaac Newton Institute of Chile, Yugoslavia Branch (Casilla 8-9, Correo 9, Santiago, Chile)*

<sup>4</sup>*Instituto de Astrofísica de Canarias C/ Vía Láctea, s/n E38200 - La Laguna (Tenerife), Spain*

1popovic@aob.bg.ac.yu

## ABSTRACT

We have studied the Ly $\alpha$ , H $\beta$ , H $\alpha$  and Mg II $\lambda 2798$  line profiles of the Seyfert 1 galaxy III Zw 2. The shapes of these broad emission lines show evidence of a multicomponent origin and also features which may be identified as the peaks due to a rotating disk. We have proposed a two-component Broad Line Region (BLR) model consisting of an inner Keplerian relativistic disk and an outer structure surrounding the disk. The results of the fitting of the four Broad Emission Lines (BELs) here considered, are highly consistent in both the inner and outer component parameters. Adopting a mass of  $\sim 2 \cdot 10^8 M_\odot$  for the central object we found that the outer radius of the disk is approximately equal for the four considered lines ( $\sim 0.01$  pc). However, the inner radius of the disk is not the same: 0.0018 pc for Ly $\alpha$ , 0.0027 pc for Mg II, and 0.0038 pc for the Balmer lines. This as well as the relatively broad component present in the blue wings of the narrow [OIII] lines indicate stratification in the emission-line region. Using long-term H $\beta$  observations (1972-1990, 1998) we found a flux variation of the BEL with respect to the [OIII] lines.

*Subject headings:* galaxies: individual (Mrk1501) – galaxies: Seyfert – line: profiles – accretion disks

## 1. Introduction

The active galaxy III Zw 2 (Mrk 1501) appears to be essentially stellar-like, with faint wisps extending toward the northwest (Arp 1968, Zwicky 1971). III Zw 2 presents the classic broad emission line characteristic of a type 1 Seyfert galaxy or a quasar (Arp 1968, Sargent 1970, Khachikian & Weedman 1974, Osterbrock 1977). The emission lines of III Zw 2 have been studied in several papers (Osterbrock 1977, Kaastra & Korte 1988, Corbin & Borson 1996). Crenshaw et al. (1999) noted the presence of intrinsic absorption lines in the ultraviolet spectrum of III Zw 2 obtained with the Hubble Space Telescope (HST).

A disk model for the broad emission-line region of III Zw 2 has been proposed in several papers (Kaastra & Korte 1988, Corbin & Borson 1996, Shimura & Takahara 1995, Rokaki & Boisson 1999). The rotating accretion disk model (van Groningen 1983, Kaastra & Korte 1988, Perez et al. 1988, Chen et al. 1989, Chen & Halpern 1989, Halpern 1990, Eracleous & Halpern 1994, Pariev & Bromley 1998, Rokaki & Boisson 1999, Shapovalova et al. 2001, Popović et al. 2002, Kollatschny & Bischoff 2002) has been very often discussed in order to explain the observed broad optical emission-line profiles in AGN. This model fits well the widely accepted AGN paradigm in that the 'central engine' consists of a massive black hole fueled by an accretion disk. However, the fraction of AGN with double-peaked lines (which may indicate the disk emission in a line) is small, and the observational evidence to support the existence of a disk is not statistically significant.

Observations in a wide band of wavelengths (X-ray, UV, optical) also indicate that an accretion disk could be present in III Zw 2. In particular, Kaastra and Korte (1988) gave some parameters for the central engine. They hold that the accretion disk has a large thickness in the central part, that it probably extends to 0.2 pc and that the central black hole has a mass of about  $5 \cdot 10^7 M_\odot$ . From the study of the emission lines, Kaastra & Korte inferred dimensions of  $\sim 7 \cdot 10^{18}$  m and  $\sim 10^{16}$  m for the NLR and the BLR, respectively. Shimura and Takahara (1995) reproduced the specific UV and soft X-ray luminosities in III Zw 2 from a disk emission spectrum. More recently, Rokaki & Boisson (1999) show that the UV continuum and the H $\beta$  line emission are compatible with an accretion disk model.

The aim of this paper is to analyze the shapes of the Hydrogen and Mg II $\lambda 2798$  emission lines of III Zw 2 in order to identify features which may be associated with the emission from a rotating disk and try to find evidence that suggests that disk emission can contribute to line emission. We propose a structure for the BLR which can describe the shape of these lines. We also use a set of observations of the H $\beta$  line, taken over a long period of time, to discuss the H $\beta$  line shape variability.

## 2. Observations and data reduction

We use spectra of III Zw 2 taken from three sources: (i) 38 spectra including the H $\beta$  line (wavelength interval 4750-5900 Å) observed at the Crimean Astrophysical Observatory (CrAO) by K.K. Chuvaev with the 2.6 m Shain telescope during the period 1972-1990 (HJD 2441361 till 2448153), (ii) spectra taken with the HST in 1992 which include the Ly $\alpha$  and MgII $\lambda$ 2798 lines, and (iii) 3 spectra taken in 1998 with the Isaac Newton Telescope (INT) at La Palma Observatory including the H $\alpha$  and H $\beta$  lines.

The spectra including the Ly $\alpha$  and MgII $\lambda$ 2798 lines were also observed on January 18, 1992 with the HST Faint Object Spectrograph (FOS). Two different gratings were used to cover the wavelength range around the Ly $\alpha$  and Mg II $\lambda$ 2798 lines: a) G130H in the spectral range from 1087.23 Å to 1605.52 Å with spectral resolution of 0.98 Å; and b) G270H in the spectral range from 2221.10 Å to 3300.10 Å with spectral resolution of 2.05 Å. Three spectra of Ly $\alpha$  and one of Mg II $\lambda$ 2798 were taken. The spectra have been reduced by the HST team, and are in the format intensity vs. wavelength. We obtained an averaged spectrum of Ly $\alpha$  from the three observed.

At the CrAO, 38 spectra including the H $\beta$  line (wavelength interval 4750-5900 Å) were obtained with the 2.6 m Shain telescope during the period 1972-1990. The spectral resolution was  $\sim 8$  Å. The spectrograph slit and seeing were in the 1.8'' – 2.0'', and 2'' – 3'' ranges, respectively. The spectra of H $\beta$  were scanned with a two-coordinate CrAO microphotometer (as in the case of Akn 120, see e.g. Stanić et al. 2000, Popović et al., 2001). The reduction procedure includes corrections for the film sensitivity, sky background, and instrumental spectral sensitivity. The wavelength and flux calibration were made using the SPE data reduction package, developed by S.G. Sergeev. The wavelength calibration was based on the night sky lines and narrow emission lines of the galaxy. The spectra have been normalized to the [OIII] $\lambda$ 5007 emission line flux.

H $\alpha$  and additional H $\beta$  observations were performed on August 7, 1998 with the 2.5 m INT at La Palma. We used the Intermediate Dispersion Spectrograph (IDS) and the 235 camera in combination with the R1200Y grating. Two exposures of 1800 and 825 s, respectively, included H $\beta$  and another one of 1800 s included H $\alpha$ . The seeing was 1''.1 and the slit width 1''.5. The spectral resolution was 1.8 Å. Standard reduction procedures including flat-fielding, wavelength calibration, spectral response, and sky subtraction were performed with the help of the IRAF software package.

The red-shift of III Zw 2 was taken to be  $z=0.0898$  (Véron-Cetty & Véron 2000).

### 3. Gaussian analysis

#### 3.1. Line profile analysis

The first step in analyzing the emission lines was to define the continuum. In the case of H $\beta$  the local continuum in four narrow zones around 4800, 4900, 5520 and 5600 Å was fit with a second order polynomial. For the H $\alpha$ , Ly $\alpha$  and Mg II $\lambda 2798$  lines the continuum was estimated using a straight line between two wavelengths: around 6900 Å and 7400 Å for H $\alpha$ ; 1200 Å and 1450 Å for Ly $\alpha$ ; and 2900 Å and 3200 Å for the Mg II line. We fit each line with a sum of Gaussian components using a  $\chi^2$  minimalization routine to obtain the best fit parameters. We have also assumed that the narrow emission lines can be represented by one or more Gaussian components (see text below). In the fitting procedure, we look for the minimal number of Gaussian components needed to fit the lines. It was found that three broad Gaussian components provides a good fit to the profiles of the Ly $\alpha$  and Mg II lines, while one additional narrow component was needed to fit the Balmer lines.

In Figs. 1–5 we can recognize clear evidence of substructure in all the BELs. In the line profile with highest resolution (the H $\beta$  spectrum from the INT, see Fig. 1), the narrow emission line is blue-shifted with respect to the BEL which exhibits a gentle slope towards the red and a steeper drop towards the blue. Asymmetries are also present in the H $\alpha$ , Ly $\alpha$  and MgII BELs (Figs. 2–4). The absence of a narrow emission-line component in the Ly $\alpha$  and MgII lines indicates that the contribution of the Narrow Line Region emission in these lines is minor.

##### 3.1.1. H $\beta$

To study in more detail the presence of substructure we performed a multi-Gaussian fit to the INT high resolution H $\beta$  line profile. The low resolution and low S/N ratio of CrAO spectra could not be qualitatively decomposed into Gaussian components and we use the spectra only for line variation investigation (see Sec. 4). To limit the number of free parameters in the fit we have set some *a priori* constraints (Popović et al. 2001, 2002). In the first place, the three narrow Gaussians representing the two [OIII] $\lambda\lambda 4959, 5007$  lines and the narrow H $\beta$  component are fixed at the same red-shift with Gaussian widths proportional to their wavelengths. Full Width at Half Maximum (FWHM) is connected with width of the Gaussian profile (W) as  $FWHM = 2W\sqrt{\ln 2}$ . Second, we have linked the intensity ratio of the two [OIII] lines according to the line strengths, 1:3.03 (Wiese et al. 1966). Finally, we have included in the fit a red shelf Fe II template consisting of nine Fe II lines belonging to the multiplets 25, 36 and 42 (Korista 1992). We took the relative strength of these lines

from Korista (1992) and supposed that all the Fe II lines originated in the same region, that is, all of them have the same red-shift and widths proportional to their wavelengths.

We obtained reasonably good fits by considering the above mentioned narrow and shelf components and three broad  $H\beta$  components with red-shifts: 0.0856 ( $W=2200$  km/s), 0.0898 ( $W=1900$  km/s) and 0.0950 ( $W=2800$  km/s), see Fig. 1. The central broad component is relatively weak and, in principle, consistent fittings can be obtained with only two broad components on the basis of minimal Gaussian component assumption. Therefore we used F-test (Eadie et al. 1971) in order to compare the  $\chi^2$  of two and three broad Gaussian models and find that the model with the central component leads to a significant improvement in fit quality at the 99.8% confidence level. On the other hand, as we will see, the central component is present in the other hydrogen and MgII lines in the same way.

We have also used the high resolution spectra from the INT to study in detail the [OIII] lines. To do this we have subtracted from the original spectrum all the  $H\beta$  components (broad and narrow) and the Fe II shelf, obtaining the spectrum shown in Fig. 5. In this Figure we note that both [OIII] lines show very extended wings and can not properly be fitted by a Gaussian. We also notice that the wings are asymmetrical, being more gently sloped towards the blue. We have performed a multi-Gaussian fit to these lines finding that at least one relatively broad ( $W = 410$  km/s) and blue-shifted (0.0875) component should be included to account for the extended wings (see Fig. 5). One can expect that other narrow lines in the optical spectra have the same shape as the [OIII] ones and that the [OIII] line profile can be used as template to fit these lines. But taking into account that the other narrow lines are very weak in comparison with the corresponding broad one (see e.g. [NII] in the  $H\alpha$  wavelength region) the asymmetry seen in [OIII] will not affect significantly to the line profile and for the purposes of the paper the narrow lines can be satisfactorily fitted with one single Gaussian. On the other hand we can not be sure that all the narrow lines are emitted under the same kinematical and physical conditions.

### 3.1.2. $H\alpha$

To fit the  $H\alpha$  line, we have assumed that the [NII] $\lambda\lambda 6548, 6583$  and the  $H\alpha$  narrow component have the same red-shift and Gaussian widths proportional to their wavelengths. Taking into account that the two [NII] lines belong to the transition within the same multiplet we assume an intensity ratio of 1:2.96 (see e.g. Wiese et al. 1966). However, a simple inspection to Fig. 2 shows that the peak of the [NII] $\lambda 6548$  line is higher than the peak of the [NII] $\lambda 6583$  line. This may indicate the presence of a blue-ward asymmetric underlying component. We have been only partially successful in reproducing the narrow [NII] $\lambda 6548$

line. This is not very important at this stage but we will need to clean it from the line profile to fit the disk model in §5. For this reason we have considered an additional arbitrary narrow component at  $\lambda 6548$  to totally remove this line.

In this case we also found good fits using in addition to these narrow components, three broad components for  $H\alpha$  (see Fig. 2). As in the  $H\beta$  case there is a central broad component ( $z=0.0898$ ,  $W = 1250$  km/s) located between two other broad components, red-shifted ( $z=0.095$ ,  $W = 2500$  km/s) and blue-shifted ( $z=0.0861$ ,  $W = 2330$  km/s) ones. In the case of  $H\alpha$ , the broad central component contributes a larger fraction of the integrated emission-line flux than does the corresponding component in  $H\beta$ .

### 3.1.3. $Ly\alpha$

The complex  $Ly\alpha$  shape contains three absorption lines and two narrow emission lines, Fig. 3. In order to clean the absorption lines as well as the emission satellite lines we assume that each one of them can be represented by a Gaussian. The central absorption line is red-shifted around 0.0888 and probably arises from a  $Ly\alpha$  auto-absorption. The feature at  $\lambda \approx 1335$  Å is possibly an intrinsic NV absorption (Crenshaw et al. 1999). The very weak absorption component in the blue wing may be the  $SiIII\lambda 1207$  line (see e.g. Laor et al. 1994, 1995). The two narrow emission lines in the blue wing are very close to the  $SiII\lambda 1195, 1197$  lines (Laor et al. 1994, 1995), but the observed line profiles are too narrow, that would not be expected for these permitted Si transitions. This feature can be identified as contribution of geocoronal  $OI\lambda 1302, 1306$  emission lines (see Eracleous 1998). The lines were fitted with two Gaussian and subtracted from the  $Ly\alpha$  blue wing.

In the red wing of the  $Ly\alpha$  line there appear the  $NV\lambda\lambda 1239, 1243$  lines (Wilkes & Carswell 1982, Buson & Ulrich 1990, Laor et al. 1994, 1995). In order to subtract these lines we supposed that they come from the same emission region, i.e. that they have the same  $w/\lambda$  and intensity ratio  $I(1238)/I(1242)=1.98$  (Wiese et al. 1966).

We needed three broad components to perform the multi-Gaussian fitting of the  $Ly\alpha$  line (Fig. 3) with parameters:  $W \approx 3150$  km/s,  $z \approx 0.083$ ;  $W \approx 1380$  km/s,  $z \approx 0.0898$ , and  $W \approx 3250$  km/s,  $z \approx 0.0943$ . The width and red-shift of the Gaussians fitted to the NV lines were 2270 km/s and  $z \approx 0.0898$ , respectively. The estimated ratio of  $I(NV)/I(Ly\alpha)$  is around 0.12, in a very good agreement with previous estimates (Laor et al. 1994, 1995).

### 3.1.4. $MgII\lambda 2798$

The contribution of 33 Fe II lines from multiplets 60, 61, 62 and 63 to the red and blue wing of  $MgII\lambda 2798$  has been taken into account. We assume that line intensities ratio within a multiplet is proportional to the ratio of corresponding line strengths. The atomic data for the line strength we took from the NIST web site (<http://physics.nist.gov/cgi-bin/AtData>). We also assume that the Fe II emission originates in the same region, i.e. the lines have the same width and shift. The decomposition of  $MgII\lambda 2798$  is shown in Fig 4. The scaled and broadened Fe II template is indicated by the dashed lines (bottom). As in the case of the  $H\beta$ ,  $H\alpha$  and the  $Ly\alpha$  lines, the  $MgII$  line can be decomposed into three broad Gaussian components (Fig. 4) with parameters:  $W \approx 2700$  km/s,  $z \approx 0.0843$ ;  $W \approx 1450$  km/s,  $z \approx 0.0896$ ; and  $W \approx 3600$  km/s,  $z \approx 0.0980$ . The lines from the Fe II template have  $W = 2100$  km/s,  $z = 0.0898$ .

## 3.2. Discussion of the multi-Gaussian analysis

In Fig. 6 we present the width of the different broad components versus their centroid velocities (relative to the systemic one). The different components appear well separated in this diagram, showing the consistency of the multi-Gaussian decomposition. By inspection of the diagram we can derive the following conclusions:

- (i) the best fit with Gaussian functions can be obtained only if we use three broad Gaussians.
- (ii) the Gaussian decomposition indicates the existence of a central broad component of red-shift consistent with the systemic velocity.
- (iii) the presence of red- and blue-shifted broad components in the case of all considered lines suggests that part of the emission may originate in a different region, possibly a disk.

If we assume that a disk (or a disk-like) region exists, we can roughly estimate the parameters of the disk using the results of Gaussian analysis and the relationship (see Popović et al. 2002)

$$\sin i \approx \Delta z \sqrt{R_{\text{out}}},$$

where  $i$  is the inclination of the disk,  $R_{\text{out}}$  is outer radius given in Schwarzschild radii ( $R_{\text{Sch}} = 2GM/c^2$ ). Taking into account that  $\sin i \leq 1$ , we can estimate the maximal outer radius. From our analysis we find that  $\Delta z = z_R - z_B$  (where  $z_R$  and  $z_B$  are the shift of the red

and blue Gaussians, respectively) is in the interval from 0.0086 (for  $\text{H}\alpha$ ) to 0.014 (for Mg II 2798 line). Then we can estimate the maximal outer radius,  $R_{\text{out}}^{\text{max}} < 10^4 R_{\text{Sch}}$ . On the other hand, if we accept from previous investigations (e.g. Wandel et al. 1999, Kaspi et al. 2000, Popović et al. 2001, 2002) that the outer radius of a BLR has typical dimensions of  $\sim 1000 R_{\text{Sch}}$ , we estimate that  $i \sim 10^\circ - 20^\circ$ . This can be used as a starting point in analyzing the line shapes using a more complex model of the BLR. The inclination obtained by us is significantly smaller than the one obtained by Rokaki and Boisson (1999) for III Zw 2, but at the same time it is in agreement with a mean value of disk inclination of 21 Sy 1 galaxies given by these authors, as well as with their conclusion that "we tend to observe the Sy 1 galaxies at a more face-on inclination" (Rokaki and Boisson 1999).

#### 4. Variability

We have used the long-term  $\text{H}\beta$  observations to discuss the variability of the BELs. With this aim we have removed from each observed spectrum its continuum and used the emission in the narrow  $[\text{OIII}]\lambda 5007$  line to normalize the spectra. The high-resolution spectrum obtained with the INT, has been smoothed to match spectral resolution of the CrAO spectra. Five spectra of low S/N were rejected from the whole set.

To find any variation in the  $\text{H}\beta$  line profile along the observed period we constructed profiles of the mean, of the RMS, and of the RMS divided by the square root of the mean (Figures 7abc). As one can see in Fig. 7a the mean profile is single peaked and asymmetric with traces of shoulders in the blue and red wings which may represent substructure connected with emission from a disk. The shoulders appear clearly enhanced in Figure 7b; a more prominent one at  $X \sim -0.008$  and the other two maxima at  $X \sim 0.006$  and  $0.012$ , respectively ( $X = (\lambda - \lambda_0)/\lambda_0$ ). According to Figure 7c the highest variations are found in the region including these features between approximately  $X = -0.01$  and  $X = 0.013$ . In principle, a part of the variability in the red part of the  $\text{H}\beta$  emission line might be attributable to changes in the Fe II contribution, however we do not find evidences of variability in the stronger Fe II component beneath  $[\text{OIII}]$  (see Figs. 7bc). Leaving aside the  $\text{H}\beta$  profile, the strong dispersion in the residual He II line at  $X \sim -0.018$  is noticeable.

In order to study the line flux variation during the observed period, we have presented in Figure 8a the integrated flux ( $\text{H}\beta$  plus  $[\text{OIII}]$ , Fe II and He II lines) between  $4750\text{\AA}$  and  $5050\text{\AA}$  (rest wavelengths) for each one of the individual spectra. The resulting integrated light curve decreases a  $\sim 50\%$  from 1972 to 1998. To improve the S/N ratio we have considered seven sets of spectra (defined according to the observational gaps, see Figure 8a) averaging the spectra within each set. The averaged light curve (Fig. 8b) reproduces the variation inferred

from the individual spectra and is in good qualitative agreement with the slowly decreasing trend found by Salvi et al. in the optical B-band (see Fig. 7 in Salvi et al. 2002).

To study the flux variation of different parts of the line we have applied to the seven averaged spectra the same Gaussian analysis made in §3.1.1. To improve the fits we have, in first place, fitted the mean  $H\beta$  profile obtaining centroids for the three broad Gaussians: central ( $\sim 0.0893$ ) blue-shifted ( $\sim 0.084$ ) and red-shifted ( $\sim 0.0953$ ); similar to the ones obtained from the INT  $H\beta$  profile (§3.3.1.). In a second step we performed the Gaussian fit of the seven averaged spectra fixing the Gaussian centroids to these values. The results of this analysis can be seen in Figs. 8 and 9. In Fig. 8c we present the variation of the sum of the three Gaussians. This light curve is practically the same as the one corresponding to the integrated flux (Figure 8b). This confirms that the main contribution to the flux variation in the considered wavelength range is the variation of the  $H\beta$  broad component. In Figs. 9abc, the light curves corresponding to each one of the three Gaussian components are presented. The variation in the blue and red Gaussians (with an amplitude greater than that of the central Gaussian) tends to be correlated, once again supporting the assumption of the existence of two regions contributing differently to the  $H\beta$  broad emission line profile.

## 5. Two-component model analysis

As mentioned in the introduction, the accretion disk model was taken into consideration for III Zw 2 in previous investigations (Kaastra & Korte 1988, Shimura & Takahara 1995, Rokaki & Boisson 1999). The shape of the line profiles discussed in the present paper (two, red- and blue-shifted broad components) and our preliminary analysis also support this idea. Besides, the multi-Gaussian fitting also implies the presence of a central component with the systemic velocity. According to this result, in this section we are going to fit the lines using a two-component model based on a disk and a central Gaussian component which can be interpreted as a region surrounding the disk.

For the disk we use the Keplerian relativistic model of Chen & Halpern (1989). The emissivity of the disk as a function of radius,  $R$ , is given by  $\epsilon = \epsilon_0 R^{-p}$ .

Considering that the illumination is due to an extended source from the center of the disk and that the radiation is isotropic, the flux from the outer disk at different radii should vary as  $r^{-3}$  (Eracleous & Halpern 1994), i.e.  $p = 3$  and that is value we adopt. We express the disk dimension in gravitational radii ( $R_g = GM/c^2$ ,  $G$  being the gravitational constant,  $M$  the mass of the central black hole, and  $c$  the velocity of light). The local broadening ( $\sigma$ ) and shift ( $z_{\text{Disk}}$ ) within the disk have been taken into account (Chen & Halpern 1989), i.e.

the  $\delta$  function has been replaced by a Gaussian function (with the mentioned parameters).

Before performing the fitting we have 'cleaned' the spectra by subtracting: (i) the narrow lines from INT high-resolution  $H\beta$  and  $H\alpha$ ; (ii) the absorption features, the narrow emission in the blue wing, and the NV lines from  $Ly\alpha$ ; (iii) the narrow [OIII] lines and the Fe II template from  $H\beta$  and (iv) the Fe II template from the blue and red wing of the Mg II line. It is striking that after this operation is done, the features associated with the disk are visible not only in the asymmetrical wings of Mg II but also in the red and blue shoulders of the  $Ly\alpha$  and  $H\alpha$  as well as in the triangular shape and the red shoulder of  $H\beta$  (see Fig. 10). To compare the line profiles we present in Fig. 10a the intensities normalized to the peak ones *vs.*  $X = (\lambda - \lambda_0)/\lambda_0$ . As one can see from Fig. 10a the lines have similar shapes.

When a chi-square minimization including all the parameters at once is attempted, it is found that the results are very dependent on the initial values given to the parameters. To overcome this problem we have, in the first place, tried several values for the inclination using an averaged profile of all four lines (Fig. 10b). We found that the best che-by-eye fits can be obtained for values of  $i \approx 12^\circ$ . Accordingly we have fixed it to  $i = 12^\circ$  and performed a chi-square fitting of the other parameters starting from suitable initial values. The fit of the BELs wings strongly restricts the value of the inner radius and additional "local" broadening, i.e. random velocity of emission gas in the disk. This fact (related to the emissivity dependence,  $p \approx -3$ ) supports the validity of the determination of these parameter from the line profile fits. We note here that changing the inner (outer) radius of the disk and parameter  $p$  we can obtain a satisfactory fit with the inclination  $12^\circ \pm 5^\circ$ .

The results of the fit are presented in Fig. 10bcdef, and the disk and Gaussian parameters in Table 1. This Table enables us to point out the following results: (i) There is a very good consistency among the parameters ( $z$  and  $W$ ) of the broad components representing the region surrounding the disk. Their red-shifts exhibit a very small difference with respect to the red-shift of the [OIII] narrow lines. (ii) There is also a good consistency in the red-shifts for the disk corresponding to  $Ly\alpha$ ,  $H\alpha$ ,  $H\beta$ , and MgII. The average  $z$  for these four disk lines appears to be slightly blue-shifted (by about 600 km/s) with respect to the systemic one. (iii) The inner radius of the  $Ly\alpha$  emitting disk is clearly smaller than the others.  $H\alpha$  and  $H\beta$  exhibit a very good coincidence of the inner radii but the inner edge of the MgII emission ring seems to be closer to the disk center although this point should be viewed with caution. (iv) The disk emission component contributes more to the total flux than the low-velocity component of the BLR.

Taking into account the estimated mass of the central object in III Zw 2 ( $M \sim 2 \cdot 10^8 M_\odot$ ) given by Vestergaard (2002) we can obtain the dimensions of the radiating disk:  $R_{\text{inn}} \sim 5 \cdot 10^{13}$  m,  $R_{\text{out}} \approx 3 \cdot 10^{14}$  m. This last value is in agreement with the estimation given by Kaastra

& Korte ( $\sim 2 \cdot 10^{14}$  m). The size of the whole BLR (disk + surrounding region) cannot be inferred from this analysis but it might be considerably larger (Collin & Huré 2001). On the other hand, the BLR surrounding the disk may originate from an accretion disk wind, that may be created due to several disturbances capable of producing shocks (e.g. Bondi-Hoyl flow, stellar wind-wind collision, and turbulences, see e.g. Fromerth & Melia 2001). Also, a Keplerian disk with disk wind can produce single peaked broad emission lines (Murray & Chiang 1997). Recently, Fromerth & Melia (2001) described a scenario of the formation of BLR in the accretion disk shocks, that can create a surrounding BLR.

We should mentioned here that other geometries can contribute to the substructure seen in III Zw 2 line shapes. Besides emission of the disk (or disk-like region) or emission from spiral shock waves within a disc (Chen et al., 1989, Chen & Halpern, 1989), the following geometries may cause substructures in line profiles: i) emission from the oppositely-directed sides of a bipolar outflow (Zheng et al., 1990, Zheng et al., 1991); ii) emission from a spherical system of clouds in randomly inclined Keplerian orbits, illuminated anisotropically from the center (Goad & Wanders, 1996); and iii) emission of the binary black hole system (Gaskell, 1983, 1996). But, in any case the two-component model should be taken into account, considering a low-velocity BLR and one additional emitting region.

## 6. Conclusions

We have analyzed UV spectra and a collection of optical spectra of III Zw 2 procured in over 20 years. The flux of H $\beta$  spectra shows variability in the wings, as well as in the line core. The variation of the blue and red wing fluxes tends to correlate during the considered period. It indicates that line wings originate in the same region, while the line core arises from another emission line region (low-velocity BLR). We have also discussed the possible contribution of a Keplerian disk of emitters to the BELs, finding the following results:

1 - The shape of the BELs (especially after removing the narrow and absorption lines) indicates a multicomponent origin, and certain features –like the shoulders in Ly $\alpha$ , H $\alpha$  and H $\beta$  and the slight profile asymmetries – that can be associated with a disk.

2 - The same two-component model (Keplerian relativistic disk + a surrounding emission region) can consistently fit the 4 BELs considered here (Ly $\alpha$ , MgII, H $\beta$ , and H $\alpha$ ). This supports the standard model hypothesis in the sense that a part of the broad line emission arises from a Keplerian disk.

3 - From the fitted disk parameters and the mass of the central object (Vestergaard 2002) we can estimate that the Ly $\alpha$  disk has inner and outer radii of around 0.0018 and 0.01

pc, respectively. However, the inner radius is greater for the Mg II ( $\sim 0.0027$  pc) and for the H $\alpha$  and H $\beta$  lines ( $\sim 0.0038$  pc). This indicates a radial stratification in the disk. The relatively broad component present in the blue wings of the narrow [OIII] lines is another indication of stratification and perhaps could indicate a connection between the outer BLR and the NLR.

## 7. Acknowledgments

This work was supported by the Ministry of Science, Technologies and Development of Serbia through the project P1196 “Astrophysical Spectroscopy of Extragalactic Objects” and the project P6/88 ”Relativistic and Theoretical Astrophysics” supported by the IAC. L. Č. P. is supported by Alexander von Humboldt Foundation through the program for foreign scholars. L. Č. P. and E. B. thanks the Institute for Astrophysics Canarias for the hospitality during his stay at the Institute. We would like to thank to the anonymous referee for the very useful comments.

## REFERENCES

Arp, H. 1968, ApJ, 152, 1101.

Buson, L.M. & Ulrich, M.-H.. 1990, A&A, 240, 247.

Chen, K., Halpern, J.P. & Filippenko, A.V. 1989, ApJ, 339, 742.

Chen, K. & Halpern, J.P. 1989, ApJ, 344, 115.

Collin, S. & Huré, J.-M. 2001 A&A, 372, 50.

Corbin, M. C. & Boroson, T. A. 1996, ApJ, 107, 69.

Crenshaw, D.M., Kraemer, B.S., Boggess, A., Maran, S.P., Mushotzky, R.F., Wu, C.-C. 1999, ApJ, 516, 750.

Eadie, W.T., Drijard, D., James, F.E., Roos, M. & Sadoulet, B. 1971, Statistical Methods in Experimental Physics (Amsterdam: North-Holand)

Eracleous, M. 1988, CAL/FOS, 153, 1 (<http://www.astro.psu.edu/users/mce/preprints/calfos.pdf>)

Eracleous, M. & Halpern, J.P. 1994, ApJS, 90, 1

Fromerth, M.J. & Melia, F. 2001, ApJ, 549, 205.

Goad, M. & Wanders, I., 1996, ApJ, 469, 113.

Gaskell, C. M., 1983, Proc. 24th Liege Intern. Ap. Colloquium, Univ. de Liege, Liege, 473.

Gaskell, C. M., 1996, ApJL, 464, 107.

Halpern, J. P. 1990, ApJ, 365, L51

Kaastra, J.S., de Korte, P.A.J. 1988, A&A, 198, 16.

Kaspi, S., Smith, P.S., Netzer, H., Maoz, D., Jannuzi, B.T., Giveon, U. 2000, A&A, 533, 631.

Khachikian, E. Yc., Weedman, D.W. 1974, ApJ, 192, 581.

Kollatschny, W. & Bischoff, K. 2002, A&A, 386, L19.

Korista, K. T. 1992, ApJS, 79, 285.

Laor, A., Bahcall, J.N., Jannuzi, B. T., et al. 1994, ApJ, 420, 110.

Laor, A., Bahcall, J.N., Jannuzi, B. T., et al. 1995, ApJ, 420, 1.

Murray, N. & Chiang, J. 1997, ApJ, 474, 91.

Osterbrock, D.E. 1977, ApJ, 215, 733.

Pariev, V. I. & Bromley, B.C. 1998, ApJ, 508, 590.

Perez, E., Mediavilla, E., Penston, M. V., Tadhunter, C., Moles, M. 1988, MNRAS, 230, 353.

Popović, L. Č., Stanić, N., Kubičela, A., Bon, E., 2001 A&A, 367, 780.

Popović, L. Č., Mediavlilla, E.G., Kubičela, A., Jovanović, P. 2002, A&A, 390, 473.

Rokaki, E. & Boisson, C. 1999, MNRAS 307, 41.

Salvi, N.J., Page, J.A., Stevens, J.A., Wu, K., Mason, K.O., Aler, M.F., *et al.* 2002, MNRAS 335, 177.

Shapovalova, A. I., Burenkov, A. N., Carrasco, L., Chavushyan, V. H., Doroshenko, V. T., Dumont, A. M., Lyuty, V. M., Valds, J. R., Vlasuyk, V. V., Bochkarev, N. G., Collin, S., Legrand, F., Mikhailov, V. P., Spiridonova, O. I., Kurtanidze, O., Nikolashvili, M. G. 2001, A&A, 376, 775.

Sargent, W.L.W. 1970, *ApJ*, 160, 405.

Shimura, T. & Takahara, F. 1995, *ApJ*, 440, 610.

Stanić, N., Popović, L. Č., Kubičela, A., Bon, E. 2000, *SerAJ*, 162, 7.

van Groningen, E. 1983, *A&A*, 126, 363

Véron-Cetty, M.-P. & Véron, P. 2000, *A Catalogue of Quasars and Active Galactic Nuclei*, Sci. Report 19.

Vestergaard, M. 2002, *ApJ*, 571, 733.

Wandel, A., Peterson, B.M., Malkan, M.A. 1999, *ApJ*, 526, 579.

Wiese, W.L., Smith, M.W., Glennon, B.M. 1966, Atomic Transition Probabilities: Hydrogen Through Neon, Vol. I, NSRDS, Washington D.C.

Wilkes, B.J. & Carswell, R.F. 1982, *MNRAS*, 201, 645.

Zwicky, F. 1971, Lists of Compact Galaxies and Compact Parts of Galaxies (Pasadena: California Institute of Tehnology).

Zheng W., Binette L., Sulentic J.W., 1990, *ApJ*, 365, 115.

Zheng W., Veilleux S., Grandi S.A., 1991, *ApJ*, 381, 418.

Table 1: The parameters of disk:  $z_{\text{disk}}$  is the shift and  $\sigma$  is the Gaussian broadening term from disk indicating the random velocity in disk,  $R_{\text{inn}}$  are the inner radii,  $R_{\text{out}}$  are the outer radii. The  $z_G$  and  $W_G$  represent the parameters of the Gaussian component.  $\langle AV \rangle$  is an averaged profile (see Fig. 10b).  $F_D/F_G$  represents the ratio of the relative disk and Gaussian fluxes.

Line	$z_{\text{disk}}$	$\sigma$ (km/s)	$R_{\text{inn}}$ ( $R_g$ )	$R_{\text{out}}$ ( $R_g$ )	$z_G$	$W_G$ (km/s)	$F_D/F_G$
Ly $\alpha$	-800	850	200	900	-20	1280	1.11
Mg II $\lambda 2789$	-350	920	300	1000	-30	1100	1.86
H $\beta$	-600	920	400	1300	-130	1100	3.14
H $\alpha$	-600	850	450	1300	-120	1170	1.52
$\langle AV \rangle$	-600	890	400	1200	-120	1170	1.72

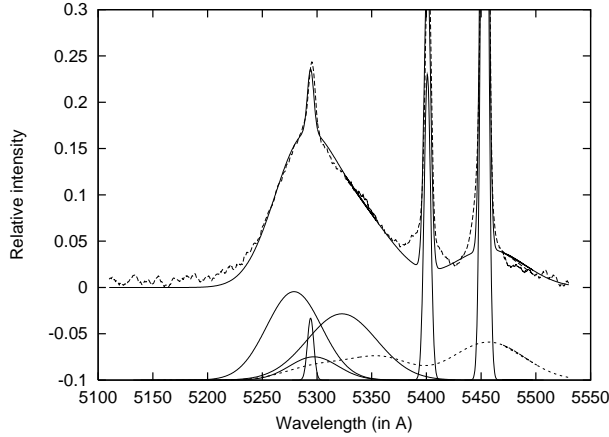


Fig. 1.— Decomposition of the H $\beta$  line observed with INT. The dashed line represents observations and solid line shows the profile obtained by Gaussian decomposition. The Gaussian components are presented at bottom. The dashed complex line, at bottom, represents the contribution of the Fe II lines

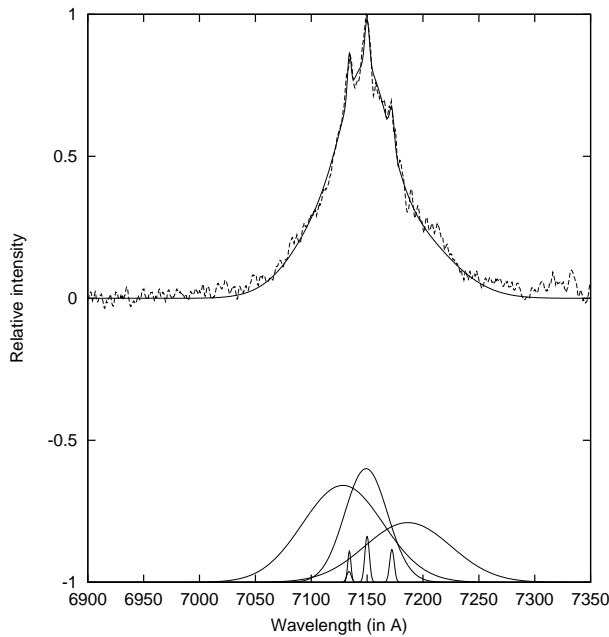


Fig. 2.— Same as in Fig. 1, but for the H $\alpha$  line. Besides the narrow H $\alpha$  central Gaussian, two weak [NII] lines have been detected: at  $\lambda\lambda 7136$  Å and  $\lambda\lambda 7174$  Å (see text for details)

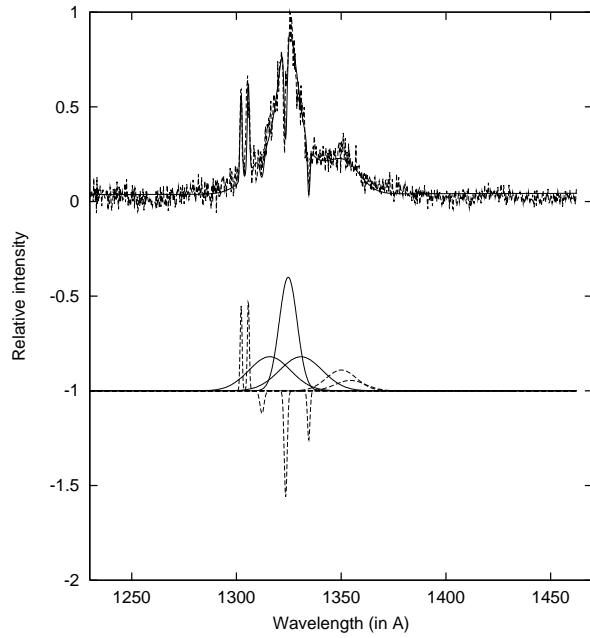


Fig. 3.— Same as in Fig. 1, but for the averaged shape of the Ly $\alpha$  line. The dashed lines, at the bottom, represent the contribution of the narrow emission and absorption lines (see text for details).

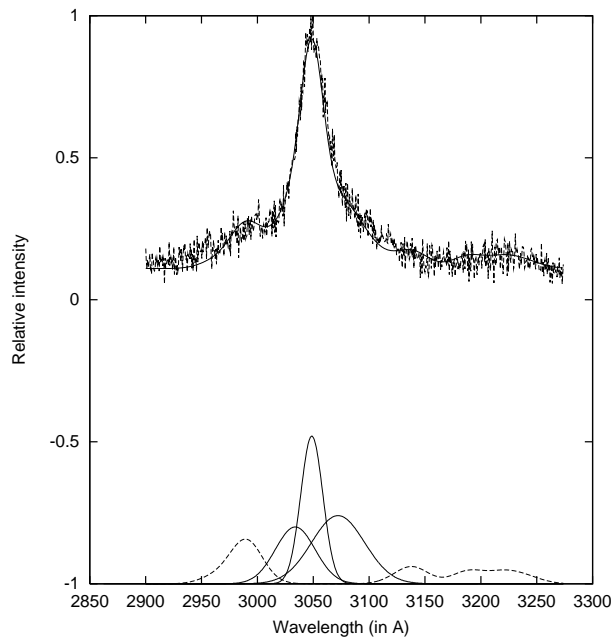


Fig. 4.— Same as in Fig. 1, but for the Mg II[2798] line. The dashed complex lines, at the bottom, represent the contribution of the Fe II template.

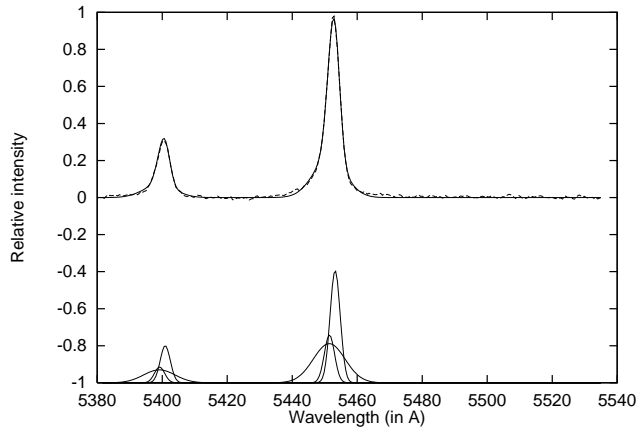


Fig. 5.— [OIII] Gaussian fitting and decomposition

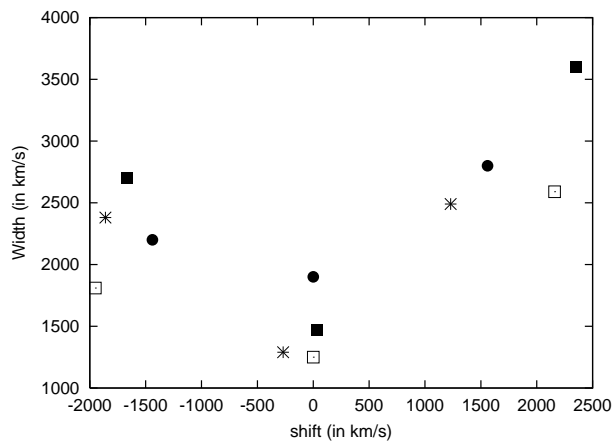


Fig. 6.— The width,  $W$ , of Gaussians as a function of the shift. The used notation is: full squares for Ly $\alpha$ , full circles for H $\beta$  observed with INT, stars for H $\alpha$  and open squares for Mg II line

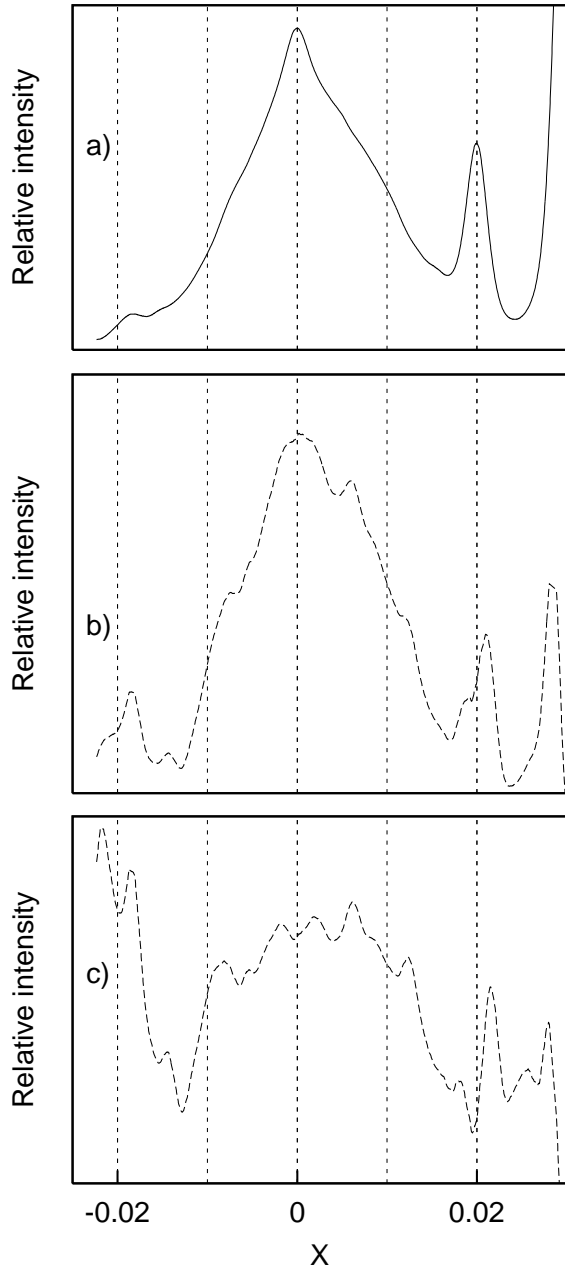


Fig. 7.— The mean  $H\beta$  line profile obtained from 34 (33 from CrAO and 1 from INT) spectra (a); the corresponding RMS profile (b) and the RMS divided by the square root of the mean profile. The intensity scale for  $H\beta$  line is from 0.0 to 0.5; for  $H\beta$  RMS is from 0.0 to 0.06 and for RMS divided by the square root of the mean profile is from 0.0 to 0.1 in units of [OIII]5007 line flux. The value  $X$  is  $(\lambda - \lambda_0)/\lambda_0$ .

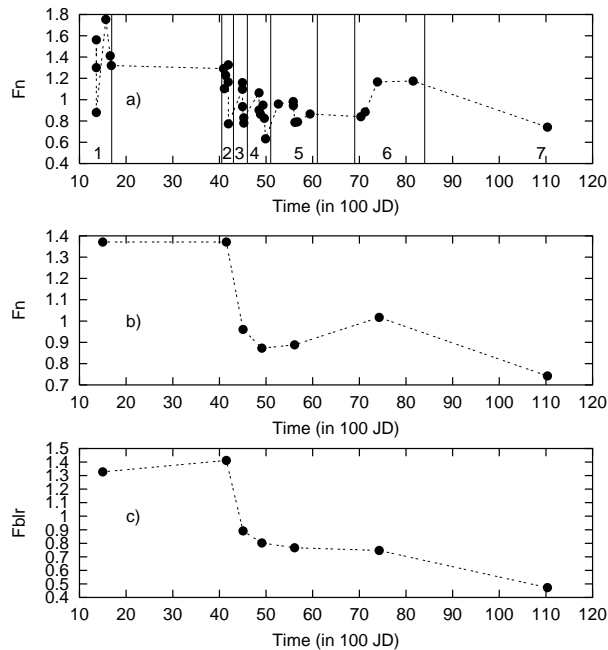


Fig. 8.— The variation of: a) the flux ( $F_n$ ) of spectra in  $H_\beta$  line region ( $H_\beta$  plus [OIII] and Fe II lines) normalized to the flux of mean spectra in  $H_\beta$  line region; b) the same variation of averaged spectra of the seven considered groups; c) the total broad line flux ( $F_{blr}$  - summ of fluxes of red, blue and central components obtained from Gaussian analysis) of seven considered groups normalized to the corresponding broad component flux of mean  $H_\beta$  line. The time is given in 100 JD, starting from the epoch 2440000 (May 23, 1968).

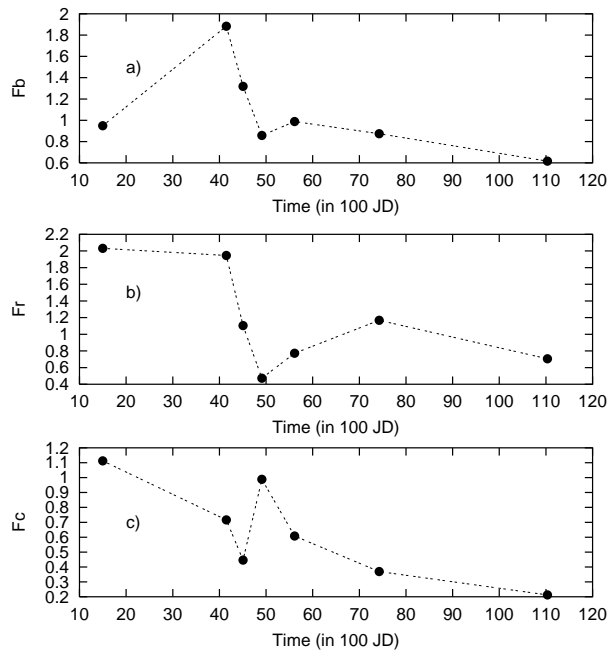


Fig. 9.— The flux variations of: (a) the blue -  $F_b$ ; (b) red  $F_r$  and (c) central -  $F_c$  H $\beta$  component normalized to the corresponding component from the mean H $\beta$  line. The time is given in 100 JD, starting from the epoch 2440000.

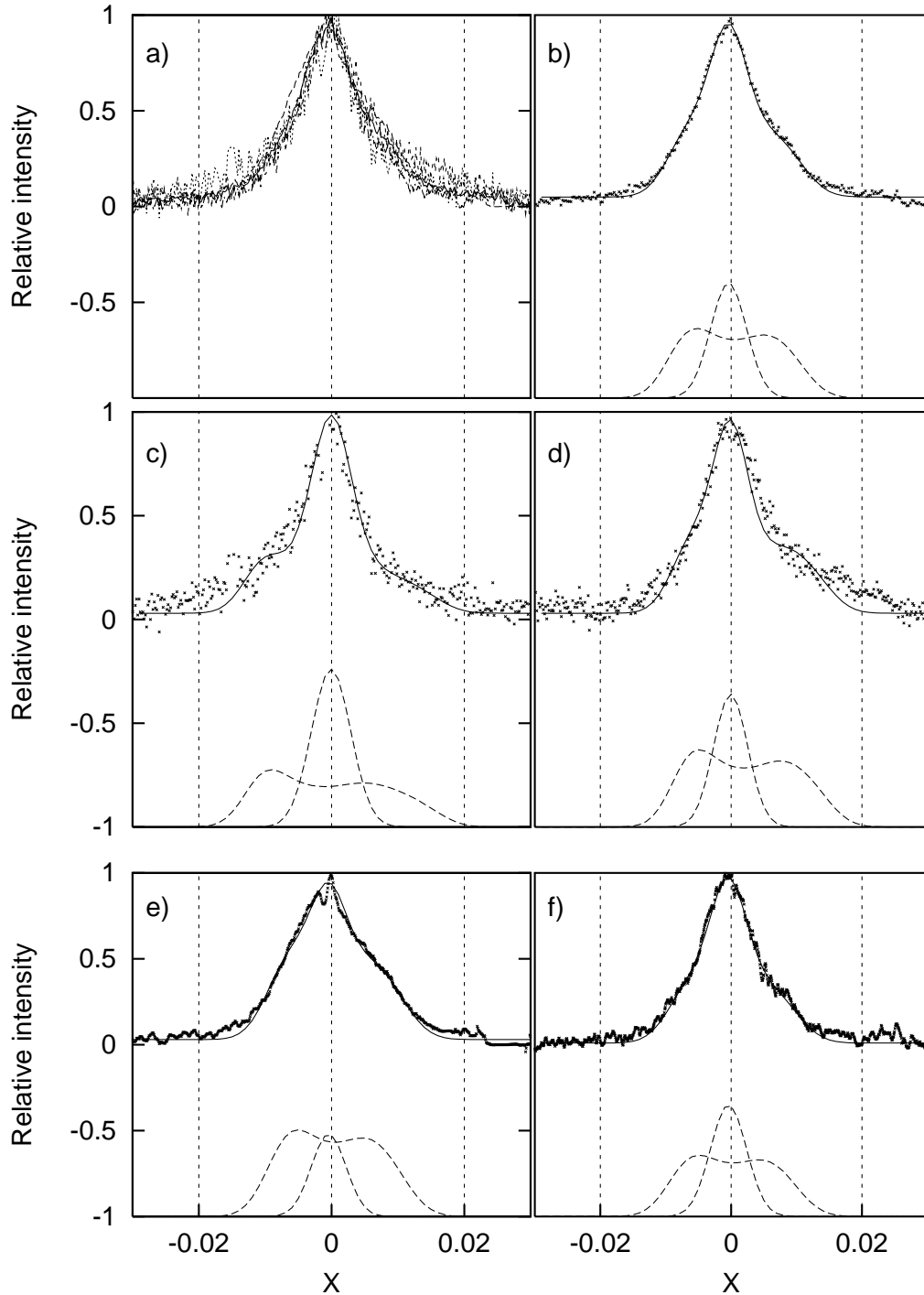


Fig. 10.— Observed lines of III Zw 2 (dots), fitted with the disk model (double-peaked) and one Gaussian; a) the comparison of all line profiles (dashed lines) with an averaged one (solid line); b) fit of the averaged line profile. Panels c,d,e,f represent fit of Ly $\alpha$ , Mg II, H $\beta$  and H $\alpha$  lines, respectively. The value  $X$  is  $(\lambda - \lambda_0)/\lambda_0$ .